HHS Public Access

Author manuscript

Genesis. Author manuscript; available in PMC 2017 January 28.

Published in final edited form as:

Genesis. 2015 September ; 53(9): 612–626. doi:10.1002/dvg.22879.

Generation of *Evc2/Limbin* global and conditional KO mice and its roles during mineralized tissue formation

Honghao Zhang[1], **Haruko Takeda**[2,3,*], **Takehito Tsuji**[4,*], **Nobuhiro Kamiya**[1,2,5,*], **Sudha Rajderkar**[1], **Ke' Ale Louie**[1], **Crystal Collier**[6], **Greg Scott**[7], **Manas Ray**[7], **Yoshiyuki Mochida**[8], **Vesa Kaartinen**[1], **Tetsuo Kunieda**[4], and **Yuji Mishina**[1,2,7]

[1]Department of Biologic and Materials Sciences, School of Dentistry, University of Michigan, MI USA

[2]Laboratory of Reproductive and Developmental Biology, National Institute of Environmental Health Sciences, National Institutes of Health, Research Triangle Park, NC 27709, USA

[3]Unit of Animal Genomics, GIGA-R & Faculty of Veterinary Medicine, University of Liège, 1 Avenue de l'Hôpital, 4000-Liège, Belgium

[4]The Graduate School of Environment and Life Science, Okayama University, Okayama City, Japan

[5]Faculty of Budo and Sport Studies, Tenri University, Nara, Japan

[6]College of Literature, Science and the Arts, University of Michigan, MI USA

[7]Knock Out Core, National Institute of Environmental Health Sciences, National Institutes of Health, Research Triangle Park, NC 27709, USA

[8]Department of Molecular and Cell Biology, Henry M. Goldman School of Dental Medicine, Boston University, 700 Albany Street, Boston, MA 02118, USA

Summary

Ellis-van Creveld (EvC) syndrome (OMIM 225500) is an autosomal recessive disease characterized with chondrodysplastic dwarfism in association with abnormalities in oral cavity. Ciliary proteins EVC and EVC2 have been identified as causative genes and they play an important role on Hedgehog signal transduction. We have also identified a causative gene *LIMBIN* for bovine chondrodysplastic dwarfism (*bcd*) that is later identified as the bovine ortholog of *EVC2*. Here, we report generation of conventional and conditional mutant *Evc2/Limbin* alleles that mimics mutations found in EvC patients and *bcd* cattle. Resulted homozygous mice showed no ciliary localization of EVC2 and EVC and displayed reduced Hedgehog signaling activity in association with skeletal and oral defects similar to the EvC patients. Cartilage-specific disruption of *Evc2/Limbin* resulted in similar but milder skeletal defects, whereas osteoblast-specific disruption did not cause overt changes in skeletal system. Neural crest-specific disruption of *Evc2/Limbin* resulted in defective incisor growth similar to that seen in conventional knockouts;

Corresponding Author: Yuji Mishina, PhD, Professor, University of Michigan, School of Dentistry, Department of Biologic and Materials Sciences, 1011 N. University Avenue, Ann Arbor, MI 48109-1078, Phone: 1-734-763-5579, Fax: 1-734-647-2110, mishina@umich.edu.

*Equal contribution

however, differentiation of amelobolasts was relatively normal in the conditional knockouts. These results showcased functions of EVC2/LIMBIN during formation of mineralized tissues. Availability of the conditional allele for this gene should facilitate further detailed analyses of the role of EVC2/LIMBIN in pathogenesis of EvC syndrome.

Keywords

Evc2; *Limbin*; mouse; primary cilium

INTRODUCTION

The Ellis-van Creveld (EvC) syndrome (OMIM 225500, also known as chondroectodermal dysplasia) is an autosomal recessive disease characterized with chondrodysplasia and dwarfism (McKusick et al. 1964; Baujat and Le Merrer 2007). EvC syndrome is a rare disease with occurrence of about 1 in 60,000. The affected individuals show a wide spectrum of developmental defects including shortening of the limbs, short ribs that result in difficulties in breathing, shortened tongue, dysplastic fingernails and postaxial polydactyly. The EvC patients have a short lip bound by the frena to the alveolar ridge, also been described as hyperplastic frenum with a shallow labial sulcus, unique to this syndrome (Priolo and Lagana 2001). About two thirds of EvC patients have mutations in either *EVC* or *EVC2* gene, both of which are located in the human chromosome 4p in a head-to-head configuration (Ruiz-Perez et al. 2000; Ruiz-Perez et al. 2003; Tompson et al. 2007). The majority of the mutations cause premature terminations of the encoded proteins. We have previously identified a causative gene, *LIMBIN* for bovine chondrodysplastic dwarfism (*bcd*) found in the Japanese brown cattle (Takeda et al. 2002). *LIMBIN* was later identified as the bovine ortholog of *EVC2*. *EVC2* have also been reported as a causative gene of chondrodysplastic dwarfism in Tyrolean grey cattle (Murgiano et al. 2014) further indicating the significance of EVC2 protein function in skeletogenesis.

Structures of EVC and EVC2 are very different and no apparent domains that can predict functions are present in either of the genes, however, these proteins form complex and co-localize at the bottom of cilia (Blair et al. 2011). Based on their ciliary localization, an involvement of EVC and EVC2 in the Hedgehog signaling has been speculated. Both *Evc* and *Evc2* mutant mice have been generated by deleting exon 1 that showed dwarfism with reduced Hedgehog signaling (Ruiz-Perez et al. 2007; Pacheco et al. 2012; Caparros-Martin et al. 2013). Mechanistic studies indicated that induction of Hedgehog signaling requires an interaction between the EVC/EVC2 protein complex and Smoothened (SMO) at the bottom of primary cilium (Dorn et al. 2012; Yang et al. 2012; Caparros-Martin et al. 2013).

In contrast to EvC syndrome, which is an autosomal recessive disorder, Weyers acrofacial dysostosis (also known as Curry-Hall syndrome, WCH) also caused by mutations in *EVC2*, is a dominant disorder (Ruiz-Perez and Goodship 2009). The primary phenotypic difference between WCH and EvC is the severity of the clinical phenotypes. In general, the WCH patients have less severe symptoms and lack the cardiac defects associated with EvC syndrome. Detailed structural analyses revealed that loss of 31–43 amino acids at the very

C-terminal portion of EVC2 makes these truncated protein a dominant negative (Dorn et al. 2012; Yang et al. 2012; Caparros-Martin et al. 2013). These truncated EVC2 can still localize to cilium, but deletion of 83 amino acids at the C-terminal end of EVC2 abolishes its ciliary localization (Dorn et al. 2012; Yang et al. 2012; Caparros-Martin et al. 2013). Since previously reported mouse line for *Evc2* mutation has deletion in exon 1, it is necessary to generate mutant mice resembling mutations found in EvC patients for understanding of molecular etiology.

Here, we generated a mouse line that shows a premature termination of *Evc2* at exon 12 (corresponding to human/cattle exon 14) to mimic mutations found in EvC patients (Tompson et al. 2007) and *bcd* cattle (Takeda et al. 2002). We also generated a conditional mouse line that displays premature termination of *Evc2* within exon 13 after Cre recombination. Homozygous mice for the conventional allele and the Cre recombined allele showed severe dwarfism with limb and dental anomalies similar to EvC patients. Cartilage-specific deletion of *Evc2* resulted in dwarf phenotypes and neural crest-specific deletion of *Evc2* resulted in tooth phenotypes similar but milder than those found in the conventional mutant mice. This indicates a potential animal model of this disease.

RESULTS AND DISCISSION

Generation of the premature termination allele of *Evc2/Limbin*

To study pathophysiological mechanism of how mutations in *Evc2/Limbin* lead to chondrodysplastic dwarfism, we first generated a global mutant mouse line by introduction of a premature stop codon along with an IRES-lacZ cassette into exon 12 (Fig. 1a) to mimic one of nonsense mutations identified in human patients (Tompson et al. 2007) and Japanese Brown cattle (Takeda et al. 2002). This mutation results in truncation of EVC2/LIMBIN protein at the 695th amino acid position and we named this allele as the exon12-stop allele or $Evc2^{ex12}$. After positive and negative selection with G418 and DT-A, correctly targeted ES cell clones were identified by Southern blot analysis using 5' and 3' external probes (Fig. 1b). After germline transmission of the mutation, the floxed PGK-neo cassette was removed by breeding with *Mox2*-Cre and the obtained mice heterozygous for $Evc2^{ex12}$ were used for further breeding (Fig. 1c).

Generation of the conditional allele of *Evc2/Limbin*

To further identify tissue-specific functions of EVC2/LIMBIN, we also generated a conditional allele for *Evc2/Limbin*. We used the all-in-one type vector for conditional gene targeting we previously reported (Multiple Amplicon Insertion Knock Out, MAIKO, vector) (Inagaki et al. 2008). The targeting vector was designed to introduce one *lox*P site and an *FRT-PGKneo-FRT* cassette to intron 12 and the other *lox*P site to intron 14 (Fig. 2a). By this way, exon 13 and 14 were flanked by the *lox*P sites. An alternative splicing between exons 12 and 15 will generate truncation at 156-base in exon 15, which produces a protein that is 105 amino acids longer than the truncated protein generated by the exon12-stop allele. Similarly, an alternative splicing between exon 12 and 16 will produce a truncated protein 90 amino acids longer than the one generated by the exon12-stop allele. Therefore, protein

products from the Cre-recombined allele, if present, should be abnormal and result in similar phenotypes found in homozygous exon 12-stop allele.

After positive and negative selections with G418 and DTA, correctly targeted ES cell clones were identified by Southern blot analysis using 5' and 3' external probes (Fig. 2a, b). The presence of the 3' *loxP* site was confirmed by using *Hind*III digestion and the 3' external probe (Fig. 2b). The targeted allele was designated as the *floxP+neo* (*fn*) allele. After confirmation of the germline transmission, F1 offspring heterozygous for *fn* were intercrossed to generate mice homozygous for *fn*. The resulting F2 showed the expected genotype ratio (+/+:*fn*/+:*fn*/*fn* = 11:24:15, 7 litters). In addition, F1 offspring heterozygous for *fn* were bred with *ROSA26-Flp* mice (Farley et al. 2000) to remove the neo cassette through recombination at the FRT site. Removal of the neo was confirmed by PCR (Fig. 2c). The targeted allele without the neo cassette was designated as the *floxP* (*fx*) allele. Intercrosses between mice heterozygous for the *fx* allele generated the expected ratio of the mice homozygous for *fx* (+/+:*fx*/+:*fx*/*fx* = 3:16:5, 3 litters). To verify that the loxP sites are functional, mice heterozygous for *fn* were bred with epiblast-specific *Sox2-Cre* transgenic mice (Hayashi et al. 2002), to remove the floxed exons 13 and 14. Offspring were analyzed by PCR to confirm the efficiency of Cre-mediated recombination of the floxed allele *in vivo* (Fig. 2c). The Cre-recombined allele was designated as the deleted exon (*dE*) allele.

When mice heterozygous for the *fn* allele were bred with mice heterozygous for the exon 12-stop allele, we obtained the expected number of mice for the *fn* allele over the ex12-stop allele (+/+:+/ex12:*fn*/+:*fn*/ex12 = 13:14:10:15, 8 litters). When mice homozygous for either the *fn* or *fx* allele were bred with mice heterozygous for the exon12-stop allele, we obtained the expected number of mice for the *fn* or *fx* allele over the exon12-stop allele (*fn*/+:*fn*/ex12 = 113:118:, 26 litters, *fx*/+:*fx*/ex12 = 72:70, 9 litters). We did not observe any significant changes in litter size or growth retardation in these mice. Taken together these results suggest that both *fn* and *fx* alleles are functional.

Functional analyses of global mutant mice for *Evc2/Limbin*

To examine *Evc2* expression pattern in the growth plate, we took advantage of the lacZ reporter knocked-in into the $Evc2^{ex12}$ allele. β-gal staining of the heterozygous $Evc2^{ex12}$ humerus indicated that *Evc2* is expressed in the growth plate cartilage, perichondrium, ossified tissues and in muscles; while, as negative control, lacZ staining on the growth plate from the $Evc2^{+/+}$ humerus did not show any positive staining (Fig. 3a, b). Similar results were also observed in the embryonic femur. These results are consistent with our previous *in situ* hybridization data on the expression pattern in the growth plate (Takeda et al. 2002).

At birth the $Evc2^{ex12/ex12}$ homozygous mutant pups were indistinguishable from their wild-type littermates (Fig. 3c). However, in a few days after birth the mutant pups started to show slower weight/length gain as evidenced by the gross picture at 1week (Fig. 3d) and 6 weeks after birth (Fig. 3e). Weekly body weight tracking indicated that both male and female $Evc2^{ex12/ex12}$ showed significantly less body weight than control littermates (Fig. 3g). Many of the mutant mice died before reaching a weaning stage (3 weeks after birth) and survivors beyond weaning were euthanized by 6 weeks after birth due to humane care. The skeleton preparation at 4 weeks indicated that $Evc2^{ex12/ex12}$ mice had smaller body length, smaller

head and even smaller arms and legs (Fig. 3f). Despite no body length differences between control and *Evc2*$^{ex12/ex12}$ at newborn stage, in *Evc2*$^{ex12/ex12}$ both forelimbs and hindlimbs were unproportionally shorter compared to litter mate control (Fig. 3h). Quantification on the length showed 15% to 30% decrease for each bone in both legs in *Evc2*$^{ex12/ex12}$ (Fig. 3i).

We bred *Evc2*$^{fx/fx}$ mice with *Sox2*-Cre mice (Hayashi et al. 2002) to obtain heterozygous mice for the Cre-recombined allele, *Evc2*$^{+/dE}$ mice, and further generated *Evc2*$^{dE/dE}$ mice. Similarly, we observed unproportionally shorter forelimbs and hindlimbs in this genotype (Fig. 3j). Quantification of the length of each appendicular bone in the limbs indicated a similar range of decrease in *Evc2*$^{dE/dE}$ as in *Evc2*$^{ex12/ex12}$ (Fig. 3k).

Premature termination of *Evc2/Limbin* abrogates ciliary localization of EVC2/LIMBIN

It was previously reported that EVC and EVC2 are ciliary proteins and their direct interaction is mutually required for their localization at the bottom of primary cilia (Blair et al. 2011). Since the ex12-stop allele can generate EVC2 protein prematurely terminated at exon 12 of *Evc2*, we examined if this truncated protein can localize to the cilia. In primary chondrocytes from wild type rib, localization of EVC2 at the bottom of primary cilium was confirmed using an antibody against N-terminal EVC2 with ciliary marker acetylated tubulin (Fig. 4a) and centrosomal marker gamma-tubulin (Fig. 4c), respectively. On the other hand, in primary chondrocytes from *Evc2*$^{ex12/ex12}$, we did not see any ciliary localization of EVC2 (Fig. 4a, c). Associated with absence of EVC2 ciliary localization, EVC also fails to localize to the bottom of primary ciliary in primary chondrocytes from *Evc2*$^{ex12/ex12}$ (Fig. 4b, d). Similarly, in primary cells from *Evc2*$^{dE/dE}$, another type of *Evc2* mutation we generated, we also observed absence of EVC2 in the primary cilium (Fig. 4e, g) associated with absence of EVC in the primary cilium as well (Fig. 4f, h). These data are consistent with previous reports indicating that deletion of 83 amino acids or more at C terminal EVC2 will abrogate ciliary localization of EVC2 and that loss of ciliary EVC2 will lead to a loss of ciliary EVC as well (Dorn et al. 2012; Caparros-Martin et al. 2013). Therefore, an early termination of the EVC2 protein in the middle of exon 12 (*Evc2*$^{ex12/ex12}$) or exon 13 (*Evc2*$^{dE/dE}$) results in a similar abrogated EVC/EVC2 ciliary function as previously reported for the *Evc2* exon1 deletion allele (Caparros-Martin et al. 2013).

To evaluate the impact of *Evc2* mutation on Hedgehog signaling induction, we isolated mouse embryonic fibroblasts (MEFs) from *Evc2*$^{ex12/ex12}$ mutants and littermate controls and induced Hedgehog signaling *in vitro* by treating cells with Sonic Hedgehog conditioned medium or SAG (Smoothen agonist). We were able to detect a robust induction of Hedgehog signaling in control MEFs, while in *Evc2*$^{ex12/ex12}$ MEFs *Ptch1* and *Gli1* induction was dramatically reduced (Fig. 4i, j). Similar results were obtained when we compared MEFs from *Evc2*$^{dE/dE}$ or *Evc2*$^{ex12/dE}$ with corresponding control cells (Fig. 4k–n). To analyze the reduced Hedgehog signaling *in vivo*, we used *Ptch1:lacZ* reporter mice (Goodrich et al. 1997). This assay verified that Hedgehog signaling levels were reduced in the humerus of the *Evc2*$^{dE/dE}$ mutants at E14.5) when compared to control littermates (Fig. 4o). Similar results were obtained when *Gli1:lacZ* reporter mice (Bai et al. 2002) were used (Fig. 4p). These results are consistent with the phenotypes found in *Evc2* null mice generated by removal of exon 1 (Caparros-Martin et al. 2013). We concluded that premature termination

of EVC2/LMBIN at exon 12 (or soon after exon 12) makes EVC2 function null and thus the floxed mouse line we generated here is a conditional null mouse line for *Evc2/Limbin*.

EVC2/LIMBIN is important for normal skeletogenesis

It is reported that Hedgehog-PTHrP feed back loop in the growth plate is playing an important role in determining the length of appendicular bones (Kronenberg 2003). Therefore, decreased Hedgehog signaling in chondrocytes within growth plates due to *Evc2* deficiency can be a reasonable cause for dwarfism in the *Evc2* mutant mice. To verify this possibility, we generated chondrocyte-specific deletion of *Evc2* by crossing *Col2:Cre ERT2*; $Evc2^{ex12/+}$ mice with $Evc2^{fx/fx}$ mice. Cre activity was induced by tamoxifen injection to pregnant mothers at E11.5 and E13.5. Beta-galactosidase staining from ROSA26 Cre reporter locus showed that more than 80% chondrocyte cells in embryonic growth plates were positive for Cre recombination (Fig. 5a). Skeletal staining with alizarin red and alcian blue indicated a decrease of limb length in chondrocyte-specific deletion of *Evc2* mutant embryos compared with control littermates (Fig. 5b). Quantification of the length of appendicular bone indicated 7% to 10% decrease for each bone when compared to that of controls (Fig. 5c), however, the phenotype was milder than that found in $Evc2^{ex12/ex12}$ or $Evc2^{dE/dE}$ mice (Fig. 3i, k).

To further dissect contribution of EVC2/LIMBIN on skeletogenesis, we compared skeletal phenotypes between global mutant mice ($Evc2^{ex12/ex12}$) and osteoblast-specific knockout of *Evc2/Limbin*. MicroCT scanning results at the newborn stage showed shorter appendicular bones in forearms in $Evc2^{ex12/ex12}$ mice (Fig. 6a, b) that is consistent with the results from skeletal staining at E18.5 (Fig. 3h). Trabecular components of tibia and femur were reduced (Fig. 6c, d) and skull bones were smaller and less mineralized especially within the nasal and frontal bones in $Evc2^{ex12/ex12}$ mice (Fig. 6e–h) when compared to those in controls. It is notable that the upper incisors were hypomorphic in the mutant mice (see next section for further analyses).

Next, we bred *Osx-GFP::Cre*; $Evc2^{ex12/+}$ mice (Rodda and McMahon 2006) with $Evc2^{fn/fn}$ mice under normal diet (thus Cre is active at the developmental stage when *Osx* is transcriptionally active) to set up osteoblast-specific disruption of *Evc2/Limbin*. In contrast, osteoblast-specific disruption of *Evc2/Limbin* did not cause overt phenotypes in skeletal system at 6 months after birth. Unlike global mutants, there were no overt differences in body weight between osteoblast-specific knockouts (cKO) and two types of controls (female; $Evc2^{fn/ex12}$;*Cre*(+), 22.46 ± 3.30 g, n=11, $Evc2^{fn/+}$;*Cre*(+), 22.87 ± 1.66 g, n=4, $Evc2^{fn/ex12}$;*Cre*(−), 23.33 ± 0.82 g, n=5, no statistic significance by Student's t-test). Lengths of long bones including femur (Fig. 6i, j) and external morphology of knee joints (Fig. 6k, l) are largely similar between cKO and controls. There were no overt changes in trabecular components and cortical components of tibia (Fig. 6m–p and data not shown) in female mice. Littermate male cKO mice also showed no statistic differences in body weight and microCT measurements of trabecular and cortical components compared with control genotypes (data not shown). These results further suggest the cause of dwarfism found in EvC patients and *Evc2* mutant mice are due to altered functions of EVC2 in chondrocytes.

These results also suggest that EVC2/LIMBIN plays an important role for craniofacial/skull development.

EVC2/LIMBIN is important for normal incisor growth

Since EvC patients manifest abnormalities in oral cavity such as missing of frontal teeth, shorter tongue and shallow sulcus with hyperplasitc frena (Priolo and Lagana 2001), we conducted phenotype analyses in the oral cavity. At 6 weeks after birth, *Evc2*$^{ex12/ex12}$ mice displayed hypomorphic incisors (Fig. 7a, b). Lateral X-ray radiogram further highlighted severely reduced upper incisor (Fig. 7f, arrowhead). *P0*- Cre was reported to specifically label neural crest derived cells (Yamauchi et al. 1999). Previous works in our lab showed that *P0*-Cre mediated recombination was also sporadically detected in the dental epithelium (Wang et al. 2011). Neural crest-specific disruption of *Evc2/Limbin* mediated by *P0*-Cre (*Evc2*$^{fn/ex12}$*;P0*-Cre (+)) resulted in similar external tooth morphology (Fig. 7d). Upper incisors were shorter than those in control littermates, but well-formed compared with those of *Evc2*$^{ex12/ex12}$ mice (Fig. 7h, arrow). Lower incisors in the neural crest-specific knockout mice of *Evc2/Limbin* showed slightly shorter length and relatively normal radio density compared with those found in *Evc2*$^{ex12/ex12}$ mice (Fig. 7f, h). Unlike *Evc2*$^{ex12/ex12}$ mice, we did not notice lethality in the neural crest-specific mutant mice during the period of observation (up to 6 months). At 6 weeks of age, the weight of *Evc2*$^{ex12/ex12}$ females was 6.57 g ± 1.24 (n=6), while the weights of *Evc2*$^{fx/ex12}$*;P0*-Cre (+) mutants and control littermates (e.g., *Evc2*$^{fx/+}$*;P0*-Cre (+)) were 13.81 g ± 4.04 (n=6) and 16.25 g ± 2.83 (n=7), respectively. The conventional mutant mice were significantly smaller ($p<0.01$) than controls, while the weight of neural crest-specific knockout mice did not significantly differ from that of controls ($p=0.29$), suggesting that the incisor phenotype may not be the primary reason of smaller body weight observed in the *Evc2*$^{ex12/ex12}$ mice. A similar external tooth phenotype was seen when *Evc2*$^{fx/ex12}$ was deleted with *Wnt1*-Cre, another neural crest-specific Cre driver (data not shown). These data suggest that loss of *Evc2/Limbin* function in dental mesenchyme partially contributes to the decreased incisor length.

In the mouse, eruption of the incisors occurs 10–12 days after birth. *P0*-Cre dependent DNA recombination was detected in the surrounding mesenchyme and sporadically in ameloblast layers in the upper incisors at E18.5 (Fig. 7q–t, green). Pre-ameloblasts located in the posterior area of normal upper incisor are less differentiated with fully extended nuclei within ameloblasts (Fig. 7q, r, blue) (Wakita and Hinrichsen 1980). As they differentiate to secretory ameloblast, the original basal side becomes apical side with nuclei polarized at the newly formed apical side (Fig. 7s, t). Histological observations of upper incisors at E18.5 revealed that ameloblasts in *Evc2*$^{ex12/ex12}$ mice did not polarize appropriately, when compared those with control littermates (Fig. 7m, n, white bars represent potion of nucleus), suggesting lack of secretory ameloblast formation in the upper incisor of *Evc2*$^{ex12/ex12}$. Consistently, the deposition of extracellular matrix proteins observed as strong pink staining in control littermates (Fig. 7m, arrowhead) was highly reduced in *Evc2*$^{ex12/ex12}$ mice (Fig. 7n). The neural crest-specific knockout mice of *Evc2/Limbin* showed comparable polarized nuclei and deposition of extracellular matrix proteins with controls at this stage (Fig. 7o, p, white bars and arrowheads). These results demonstrate that *Evc2/Limbin* is indispensable for normal incisor growth, polarization of ameloblasts and deposition of extracellular matrix

proteins. Since *P0*-Cre mediated recombination is detected mainly in dental mesenchyme and only sporadically in dental epithelium, the function of *Evc2/Limbin* in the dental mesenchyme may not be critical for ameloblast maturation or deposition of extracellular matrix proteins. We are currently analyzing the function of *Evc2/Limbin* in dental epithelium for ameloblast maturation.

Here, we report a generation of conventional and conditional *Evc2/Limbin* mutant alleles that result in premature termination of translation at (or soon after) exon 12. Resulted mice are functionally null in terms of ciliary localization of EVC2 and display similar skeletal phenotypes as those seen in the previously reported conventional mouse model (which lack sequences encoded by exon 1) (Caparros-Martin et al. 2013). In addition the primary chondrocytes isolated from our homozygote *Evc2/Limbin* mutants show reduced Hedgehog signaling activity. Similar dwarfism phenotypes found in cartilage-specific *Evc2/Limbin* mutants suggests a critical function of the gene product in chondrogenesis while its function in osteoblasts is minimal for skeletal growth. Since majority of the bones in the skull go through intramembranous ossification with minimal contribution of cartilage, it is not clear at this moment which cell types are responsible for facial phenotypes found in $Evc2^{ex12/ex12}$ mice. Comparisons of global and neural crest-specific disruption of *Evc2/Limbin* underscore importance of the gene product for normal tooth growth. Functions of EVC2/LIMBIN in dental mesenchyme are responsible for normal incisor growth, but those in other tissues may be responsible for ameloblasts maturation. Our initial analyses showcase functions of EVC2/LIMBIN in mineralized tissue formation, and thus availability of the conditional allele should facilitate further detailed analyses.

MATERIALS AND METHODS

Generation of the premature termination and lacZ knock-in mice to *Evc2/Limbin* locus

All mouse experiments were performed in accordance with institutional guidelines covering the humane care and use of animals in research. The animal protocols were approved by the Institutional Animal Care and Use Committees at the National Institute of Environmental Health Sciences and the University of Michigan. The authors are current exploring possibilities to deposit the newly developed mice to public repositories and are happy to share them upon request.

A 129/SvEv PAC mouse genomic library was screened with a probe corresponding mouse *Evc2/Limbin* exon12 that was PCR-amplified with 5'-CGCAGTCCATTACCTGCACCAG-3' and 5'-CAGTGCATCCTGCTGTAGCCTC-3' (340bp). Five positive clones were isolated, and a cosmid library was constructed from one of the PCA clones (260A19). Sixteen cosmid clones were isolated using the same probe above and the genomic organization of *Evc2/Limbin* was characterized. A 8.3-kb *Bam*HI/*Bgl*II 5' fragment and a 2.4 -kb *Bgl*II /*Bfr*I 3' fragment were used to construct a insertion gene targeting vector (Fig. 1a). A linker was added to the *Bgl*II site to introduce a stop codon (forward, 5'-GATCTTAGAGGAGCACAGCCGGGAGTCTtaa-3', reverse, 5'-TCGAttaAGACTCCCGGCTGTGCTCCTCTAA-3', the stop codon is shown in lower cases). This stop codon generates truncation of mouse EVC2/LIMBIN (Genbank, NM_145920) at 695 amino acid that is corresponding to the position where bovine LIMBIN

protein is truncated by the 2054–2055delCAinsG mutation (Takeda et al. 2002). A lacZ expression cassette following an internal ribosomal entry site and a floxed PGKneobpA cassette was inserted in forward orientation relative to the direction of *Evc2/Limbin* transcription between the two *Evc2/Limbin* regions. An MC1 DTA expression cassette was added onto the long arm of homology to enrich for homologous recombination. The targeting vector was be linearized at a unique *Xho*I site outside of the homology. Twenty five micrograms of linearized targeting vector was electroporated into 10^7 AB-2.2 ES cells that were subsequently cultured in the presence of G418 on mitotically inactivated STO fibroblasts (McMahon and Bradley 1990; Soriano et al. 1991). Six hundred G418-resistant ES clones were initially screened by Southern blotting using *Asp*718 (Isoschizomer of *Kpn*I) digested DNA and a unique 5' probe external to the region of vector homology (the probe was made by PCR using 5'-CCAGTTGGCCCCATCTCCTTTG-3' and 5'-TCCAGTTAGATGGTGCTGGAGA-3'). Correctly targeted clones were then expanded for further Southern blot analysis by *Bam*HI digestion and hybridization with a unique 3' probe external to the vector homology (the probe was made by PCR using 5'-TTGAGTATGCTATGTGTCCA-3' and 5'-CGTTCATTAAACCTCCACTACAC-3'). Twenty six correctly targeted ES clones were identified (Fig. 1b).

Three of the *Limbin*-mutant ES clones (6B6, 5A11, and 6B9) were microinjected into C57BL/6J blastocysts, and the resulting chimeric embryos were transferred to the uterine horns of day 2.5 pseudopregnant foster mothers. Chimeras were identified among the resulting progeny by their agouti fur (ES derived) and were subsequently bred with C57BL/6 mates. One of the mutant ES clones (6B6) was found to be capable of contributing to the germlines of chimeric mice. Tail DNA from the agouti pups that resulted from these matings was analyzed by Southern blot with either of the probes used to identify *Evc2/Limbin* heterozygotes for the ex12-stop allele. Mice were also genotyped by PCR amplification of tail DNA with the *Evc2/Limbin*-specific primers LbnA (5'-GAAAGTACTGCACCTCTTCACC-3') and LbnB (5'-CACTCTGGATGGTTGTGTCCT-3') and a lacZ primer, LbnC (5'-GCGGAATTCGATAGCTTGGCTG-3') (Fig. 1c). Heterozygous mice were bred with *Mox2*-Cre knock-in mice (Tallquist and Soriano 2000) to remove the floxed *PGK*-neo cassette. Removal of the cassette was confirmed by PCR with LbnB and a PGKneo primer, LbnD (5'- TTTGCACAAGGGCCCGG-3'). Following primers were used to detect presence of the PGK-neo cassette and the lacZ sequence: Neo A (5'-GGATCGGCCATTGAACAAGATGGATTGCAC-3'), Neo T (5'-CCTGATGCTCTTCGTCCAGATCATCCTGAT-3'), Z1 (5'-GCGTTACCCAACTTAATCG-3'), and Z2 (5'-TGTGAGCGAGTAACAACC-3').

Generation of the conditional mice

We PCR-amplified three specific regions of *Evc2/Limbin* mouse genome as detailed below and cloned into an all-in-one type vector named as Multiple Amplicon Insertion Knock Out (MAIKO) vector that we have previously generated (Inagaki et al. 2008). The MAIKO vector contains an FRT-PGK-neo cassette and a DTA cassette for positive and negative selection, respectively, flanked by several rare cutter enzyme sites. A 7.0-kb fragment containing exon 11 and 12 was PCR amplified from 129SvEv genomic DNA with Phusion

DNA polymerase (New England Biolabs, Inc. MA) using following primers; 5'-GTGgcgatcgcCTACAGTGGCAGGGTTACCATGGA-3' and 5'-GTGgcggccgcGCTGTTCAGatCtATCCTTCTGGAACGCACTGA-3'. *Avr*II and *Not*I sites were shown in a lower case. A 4.5-kb fragment containing exon 13 and 14 was also PCR amplified using following primers; 5'-GCGttaattaaCTCAGGTTGCAATTGACTGGCAGA-3' and 5'-CTCatcgatGAATTCCCACCTTGCCCTGAATCTCCACTT-3'. *Pac*I and *Cla*I sites were shown in a lower case. A 5.5-kb fragment containing intron 14 was PCR amplified using following primers; 5'-GTGggccggccCTTTCATCCATGGGCAGCTTCTCT-3' and 5'-GTGggcgcgccGAGAGGTTGGCTCTAGTTTGTGCT-3'. *Fse*I sites were shown in a lower case. After amplification, these fragments were digested with restriction enzymes and ligated into the corresponding sites in the MAIKO vector (Inagaki et al. 2008). The position of the probes used for Southern analysis are shown in Fig. 2a. The sizes of the restriction fragments detected by these probes in WT and targeted DNA are shown above or below the locus. A 3' *loxP* site is marked with a *Hind*III and a *Kpn*I site.

Linearized targeting vector was electroporated into 1.6×10^7 UG347 clone A3 ES cells, which we have previously established from 129SvEv blastocysts (Inagaki et al. 2008). Three hundred G418-resistant ES cell clones were initially screened by Southern blot (a unique 5'probe with *Asp*718 (Isoschizomer of *Kpn*I) digestion and a unique 3' probe with *Hind*III digestion) (Fig. 2a, b) and 13 correctly targeted ES cell clones were identified. Presence of the 3' loxP site was confirmed by genomic PCR using fxE and fxF primers (see below). The targeted ES clones (heterozygous for the floxed-neo allele, *fn*/+) were injected into blastocysts from C57BL/6 albino mice. The resulted chimeras were bred to C57BL/6 females and F1 agouti offspring were genotyped by Southern analyses. Two targeted clones were used for injection and both of them went through germline transmission (*fn*/+). They were interbred to make homozygous mice (*fn*/*fn*). The neo cassette was removed by crossing with FLPe transgenic mice to generate heterozygous mice for the floxed allele without neo (*fx*/+) (Farley et al. 2000). The resulting *Evc2*/*Limbin* mutant mice (*fx*/+) were interbred to make homozygous for the conditional allele (*fx*/*fx*) and kept on a mixed 129SvEv and C57BL6/Jax background. The floxed mice were bred with *Sox2*-Cre mice (Hayashi et al. 2002) to generate Cre-recombined allele (*dE*).

Resulted mice were genotyped by PCR. Presence of the 5' loxP site was detected with primers fxA (5'-TGTGTGGATGCACCCATGTGAC-3') and fxB (5'-GAGACTAGTGAGACGTGCTACT-3') for the *fn* allele and fxA and fxC (5'-GCTAGGCATGGCTGTGTGTA-3') for the *fx* allele (Fig. 2). Cre-dependent deletion was detected with fxA and fxD (5'-TGCATCTCCACTGGTCTCTG-3'). Presence of the 3' loxP site was detected using fxE (5'-TGTGCTGAGACAGGAACTTGG-3') and fxF (5'-CCCGGCTTGCTCAACACAGT-3').

Mouse Breeding

We used following Cre transgenic mice to breed with *Evc2*/*Limbin* conditional mice; *P0-Cre* mouse, *C57BL/6J-Tg(P0-Cre)94Imeg* (ID 148) provided by CARD, Kumamoto University, Japan (Yamauchi et al. 1999), *Osterix-Cre::GFP* mouse, *B6.Cg-Tg(Sp7-tTA,tetO-EGFP/*

cre)1Amc/J (006361) obtained from the Jackson Laboratory (Rodda and McMahon 2006), and *Col2-CreERT* mice, *FVB-Tg(Col2a1-cre/ERT)KA3Smac/J* (006774) obtained from the Jackson Laboratory (Nakamura et al. 2006). We also used lacZ knock-in mouse line to *Gli1* locus, *Gli1*^{tm2Alj}*/J* (008211) obtained form the Jackson Laboratory (Bai et al. 2002). Noon of the date when the vaginal plug observed was designated as E0.5. For *Col2-CreERT*, 75 mg/kg of tamoxifen was injected intraperitoneally at E11.5 and 13.5 to induce Cre activity.

Histology, skeletal staining, and β-gal staining

Embryos were fixed in 4% paraformaldehyde (PFA), embedded in paraffin and stained with hematoxylin and eosin (H & E) according to a standard procedure. For skeletal staining, skinned limbs were stained with alcian blue and alizarin red (Arai et al. 2002; Hayano et al. 2015). For β-gal activity, embryos were fixed with 4% PFA followed by staining with 1mg/ml of X-gal at 37°C for up to 2 days.

Isolation of primary chondrocytes and MEF, preparation of Hedgehog conditioned media, and immunocytochemistry

Rib cartilage or long bone cartilage was dissected out from newborn mice and digested by collagenase A (Roche, Indianapolis, IN, USA). Released cells were subsequently cultured in DMEM (Life Technology, Grand Island, NY, USA) with 10% FBS (Atlanta Biologicals, Flowery Branch, GA, USA). MEF cells were prepared and cultured according to previously described (Komatsu et al. 2011). Hedgehog conditioned medium was made by transfecting plasmid vector expressing N-terminal SHH into COS7 cells. Cultured primary chondrocytes were serum-starved in 0.5% serum for 36 hours and then treated with 100 ng/ml of SAG (Chemicon, Billerica, MA, USA) or cultured in Hedgehog conditioned medium for 4 hours. Cells were fixed in 4% PFA, permeabilized in PBS with 0.1% Triton x-100 (Sigma, St. Louis, MO, USA), incubated overnight at 4C with antibody against EVC2 (Y20, 1:50, Santa Cruz Biotechnology, Santa Cruz, CA, USA), EVC (HPA008703, 1:50, Sigma, St. Louis, MO, USA), Acetylated Tubulin (T6793, 1:1000, Sigma, St. Louis, MO, USA), or Gamma tubulin (T5326, 1:1000, Sigma, St. Louis, MO). Cells were then incubated with a corresponding fluorescence secondary antibody for 1 hour at room temperature and subsequently mounted by ProLong Gold antifade mountant with DAPI (P36935, Life Technology, Grand Island, NY, USA) and observed under a confocal microscope (Nikon C1).

RNA isolation and quantitative real time PCR

RNA from primary chondrocytes was isolated using TRIzol reagent (Life Technology, Grand Island, NY, USA) according to the manufacturer's instruction. Quantitative real-time PCR was performed using Applied Biosystems ViiA7, with the following Taqman probes: Mm00494645_m1 for *Gli1*, Mm00436026_m1 for *Ptch1*, and Mm99999915_g1 for *Gapdh*.

Micro Computed Tomography (μCT) Evaluation

Forearms, knee joints and whole heads from P6 mice and femora and knee joints from 6 months old mice were scanned using a μCT system (μCT100 Scanco Medical, Bassersdorf, Switzerland). Scan settings were voxel size 10 μm, medium resolution, energy 70 kV,

intensity 114 μA, 0.5 mm AL filter, and integration time 500 ms. Analysis was performed using the manufacturer's software.

ACKNOWLEDGEMENTS

We thank Dr. Kenichi Yamamura for providing *P0-Cre* mice. We also thank Drs. Susan Mackem, Andrew McMahon, Susan Dymecki, Michelle Tallquist, Alex Joyner and Phillipe Soriano for genetically modified mouse lines. We would like to express our appreciation to Tony Ward and Xixi Wang for technical assistance, Drs. Scott Barolo, Charlotte Mistretta, Noriaki Ono for helpful discussions. YMi is supported by NIH (R01DE020843 and ES071003-11), VK is supported by NIH (R01DE013085) and YMo is supported by NIH (R01DE019527). The μCT core at the School of Dentistry, University of Michigan is funded in part by NIH/NCRR S10RR026475.

LITERATURE CITED

Arai F, Ohneda O, Miyamoto T, Zhang XQ, Suda T. Mesenchymal stem cells in perichondrium express activated leukocyte cell adhesion molecule and participate in bone marrow formation. J Exp Med. 2002; 195:1549–1563. [PubMed: 12070283]

Bai CB, Auerbach W, Lee JS, Stephen D, Joyner AL. Gli2, but not Gli1, is required for initial Shh signaling and ectopic activation of the Shh pathway. Development. 2002; 129:4753–4761. [PubMed: 12361967]

Baujat G, Le Merrer M. Ellis-Van Creveld syndrome. Orphanet Journal of Rare Diseases. 2007; 2:27. [PubMed: 17547743]

Blair HJ, Tompson S, Liu YN, Campbell J, MacArthur K, Ponting CP, Ruiz-Perez VL, Goodship JA. Evc2 is a positive modulator of Hedgehog signalling that interacts with Evc at the cilia membrane and is also found in the nucleus. BMC Biol. 2011; 9:14. [PubMed: 21356043]

Caparros-Martin JA, Valencia M, Reytor E, Pacheco M, Fernandez M, Perez-Aytes A, Gean E, Lapunzina P, Peters H, Goodship JA, Ruiz-Perez VL. The ciliary Evc/Evc2 complex interacts with Smo and controls Hedgehog pathway activity in chondrocytes by regulating Sufu/Gli3 dissociation and Gli3 trafficking in primary cilia. Hum Mol Genet. 2013; 22:124–139. [PubMed: 23026747]

Dorn KV, Hughes CE, Rohatgi R. A Smoothened-Evc2 complex transduces the Hedgehog signal at primary cilia. Dev Cell. 2012; 23:823–835. [PubMed: 22981989]

Farley FW, Soriano P, Steffen LS, Dymecki SM. Widespread recombinase expression using FLPeR (flipper) mice. Genesis. 2000; 28:106–110. [PubMed: 11105051]

Goodrich LV, Milenkovic L, Higgins KM, Scott MP. Altered neural cell fates and medulloblastoma in mouse patched mutants. Science. 1997; 277:1109–1113. [PubMed: 9262482]

Hayano S, Komatsu Y, Pan H, Mishina Y. Augmented BMP signaling in the neural crest inhibits nasal cartilage morphogenesis by inducing p53-mediated apoptosis. Development. 2015; 142:1357–1367. [PubMed: 25742798]

Hayashi S, Lewis P, Pevny L, McMahon AP. Efficient gene modulation in mouse epiblast using a Sox2Cre transgenic mouse strain. Gene Expr Patterns. 2002; 2:93–97. [PubMed: 12617844]

Inagaki M, Komatsu Y, Scott G, Yamada G, Ray M, Ninomiya-Tsuji J, Mishina Y. Generation of a conditional mutant allele for Tab1 in mouse. Genesis. 2008; 46:431–439. [PubMed: 18693278]

Komatsu Y, Kaartinen V, Mishina Y. Cell cycle arrest in node cells governs ciliogenesis at the node to break left-right symmetry. Development. 2011; 138:3915–3920. [PubMed: 21831921]

Kronenberg HM. Developmental regulation of the growth plate. Nature. 2003; 423:332–336. [PubMed: 12748651]

McKusick VA, Egeland JA, Eldridge R, Krusen DE. Dwarfism in the Amish I. The Ellis-Van Creveld Syndrome. Bull Johns Hopkins Hosp. 1964; 115:306–336. [PubMed: 14217223]

McMahon AP, Bradley A. The Wnt-1 (int-1) proto-oncogene is required for development of a large region of the mouse brain. Cell. 1990; 62:1073–1085. [PubMed: 2205396]

Murgiano L, Jagannathan V, Benazzi C, Bolcato M, Brunetti B, Muscatello LV, Dittmer K, Piffer C, Gentile A, Drogemuller C. Deletion in the EVC2 gene causes chondrodysplastic dwarfism in Tyrolean Grey cattle. PLoS One. 2014; 9:e94861. [PubMed: 24733244]

Nakamura E, Nguyen MT, Mackem S. Kinetics of tamoxifen-regulated Cre activity in mice using a cartilage-specific CreER(T) to assay temporal activity windows along the proximodistal limb skeleton. Dev Dyn. 2006; 235:2603–2612. [PubMed: 16894608]

Pacheco M, Valencia M, Caparros-Martin JA, Mulero F, Goodship JA, Ruiz-Perez VL. Evc works in chondrocytes and osteoblasts to regulate multiple aspects of growth plate development in the appendicular skeleton and cranial base. Bone. 2012; 50:28–41. [PubMed: 21911092]

Priolo M, Lagana C. Ectodermal dysplasias: a new clinical-genetic classification. J Med Genet. 2001; 38:579–585. [PubMed: 11546825]

Rodda SJ, McMahon AP. Distinct roles for Hedgehog and canonical Wnt signaling in specification, differentiation and maintenance of osteoblast progenitors. Development. 2006; 133:3231–3244. [PubMed: 16854976]

Ruiz-Perez VL, Blair HJ, Rodriguez-Andres ME, Blanco MJ, Wilson A, Liu YN, Miles C, Peters H, Goodship JA. Evc is a positive mediator of Ihh-regulated bone growth that localises at the base of chondrocyte cilia. Development. 2007; 134:2903–2912. [PubMed: 17660199]

Ruiz-Perez VL, Goodship JA. Ellis-van Creveld syndrome and Weyers acrodental dysostosis are caused by cilia-mediated diminished response to hedgehog ligands. Am J Med Genet C Semin Med Genet. 2009; 151:341–351.

Ruiz-Perez VL, Ide SE, Strom TM, Lorenz B, Wilson D, Woods K, King L, Francomano C, Freisinger P, Spranger S, Marino B, Dallapiccola B, Wright M, Meitinger T, Polymeropoulos MH, Goodship J. Mutations in a new gene in Ellis-van Creveld syndrome and Weyers acrodental dysostosis. Nat Genet. 2000; 24:283–286. [PubMed: 10700184]

Ruiz-Perez VL, Tompson SW, Blair HJ, Espinoza-Valdez C, Lapunzina P, Silva EO, Hamel B, Gibbs JL, Young ID, Wright MJ, Goodship JA. Mutations in two nonhomologous genes in a head-to-head configuration cause Ellis-van Creveld syndrome. Am J Hum Genet. 2003; 72:728–732. [PubMed: 12571802]

Soriano P, Montgomery C, Geske R, Bradley A. Targeted disruption of the c-src proto-oncogene leads to osteopetrosis in mice. Cell. 1991; 64:693–702. [PubMed: 1997203]

Takeda H, Takami M, Oguni T, Tsuji T, Yoneda K, Sato H, Ihara N, Itoh T, Kata SR, Mishina Y, Womack JE, Moritomo Y, Sugimoto Y, Kunieda T. Positional cloning of the gene LIMBIN responsible for bovine chondrodysplastic dwarfism. Proc Natl Acad Sci U S A. 2002; 99:10549–10554. [PubMed: 12136126]

Tallquist MD, Soriano P. Epiblast-restricted Cre expression in MORE mice: a tool to distinguish embryonic vs. extra-embryonic gene function. Genesis. 2000; 26:113–115. [PubMed: 10686601]

Tompson SW, Ruiz-Perez VL, Blair HJ, Barton S, Navarro V, Robson JL, Wright MJ, Goodship JA. Sequencing EVC and EVC2 identifies mutations in two-thirds of Ellis-van Creveld syndrome patients. Hum Genet. 2007; 120:663–670. [PubMed: 17024374]

Wakita M, Hinrichsen K. Ultrastructure of the ameloblast-stratum intermedium border during ameloblast differentiation. Acta Anat (Basel). 1980; 108:10–29. [PubMed: 7445946]

Wang SK, Komatsu Y, Mishina Y. Potential contribution of neural crest cells to dental enamel formation. Biochem Biophys Res Commun. 2011; 415:114–119. [PubMed: 22020075]

Yamauchi Y, Abe K, Mantani A, Hitoshi Y, Suzuki M, Osuzu F, Kuratani S, Yamamura K. A novel transgenic technique that allows specific marking of the neural crest cell lineage in mice. Dev Biol. 1999; 212:191–203. [PubMed: 10419695]

Yang C, Chen W, Chen Y, Jiang J. Smoothened transduces Hedgehog signal by forming a complex with Evc/Evc2. Cell Res. 2012; 22:1593–1604. [PubMed: 22986504]

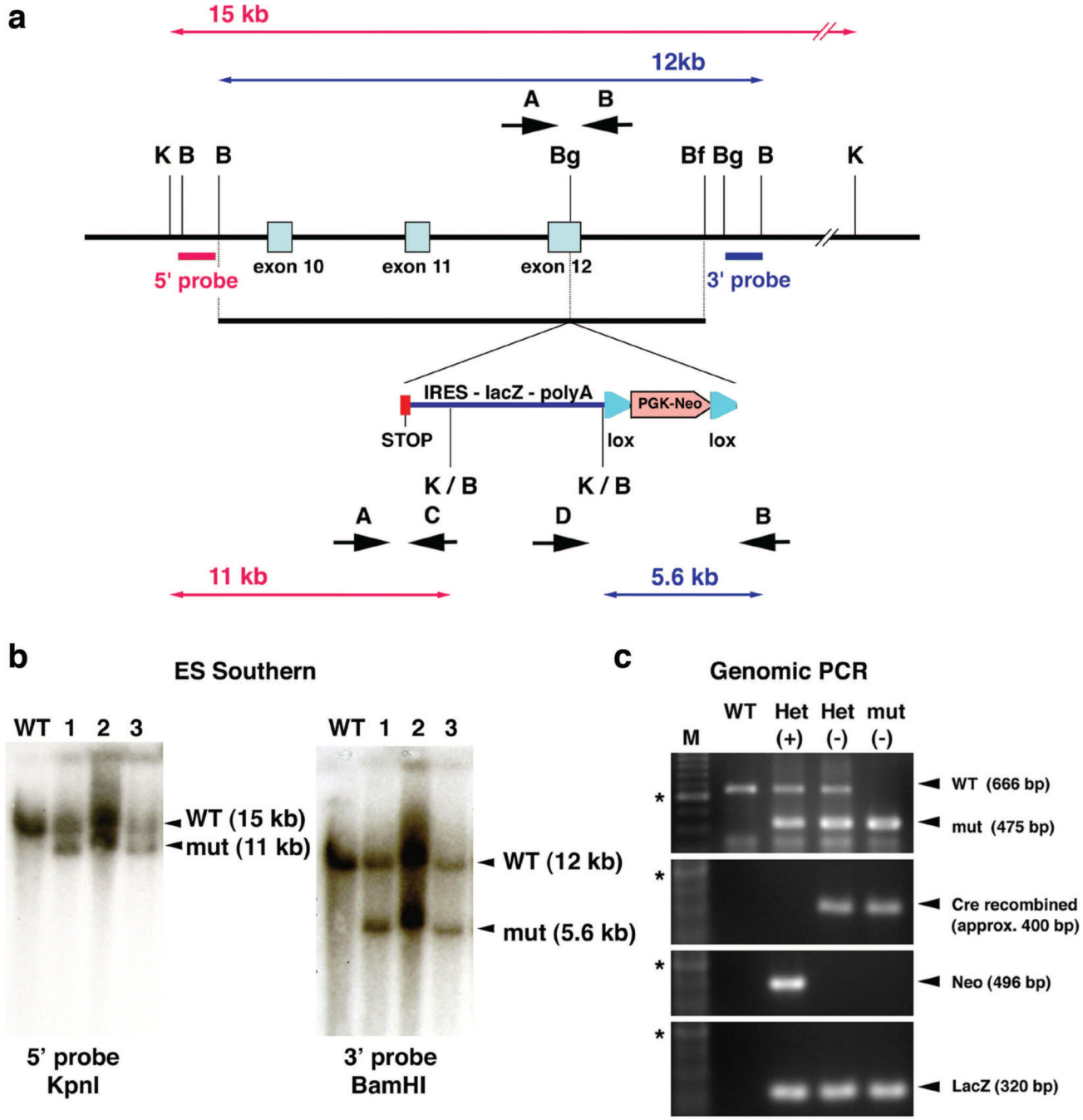

Figure 1. Generation of *Evc2/Limbin* exon-12 stop mouse

(a) A stop codon (red box) followed by an IRES-lacZ-polyA cassette and *Pgk-neo* cassette flanked by loxP sites was inserted into exon 12. Positions of 5' and 3' external probes for Southern analyses and the sizes of the restriction fragments detected by these probes are shown. B, *Bam*HI; Bf, *Bfr*I; Bg, *Bgl*II, K, *Kpn*I. Positions for PCR primers are indicated (A, B, C, D). (b) Genomic DNA from wild type ES cells (lane WT) and correctly targeted cells (lane 1–3) were digested with enzymes and blots were hybridized with probes as indicated. (c) Genomic DNA was extracted from resulted mice and primers A and B were

used to amplify WT whereas primers A and C were used to amplify the targeted allele (top). Deletion of the *Pgk-neo* cassette was confirmed by primers D and B (second top). Presence of the *Pgk-neo* cassette (second bottom) or the lacZ cassette (bottom) were confirmed using primers for each cassette. M, 100 bp ladder; *, 600 bp; (+), before deletion of the neo cassette; (−), after deletion of the neo cassette.

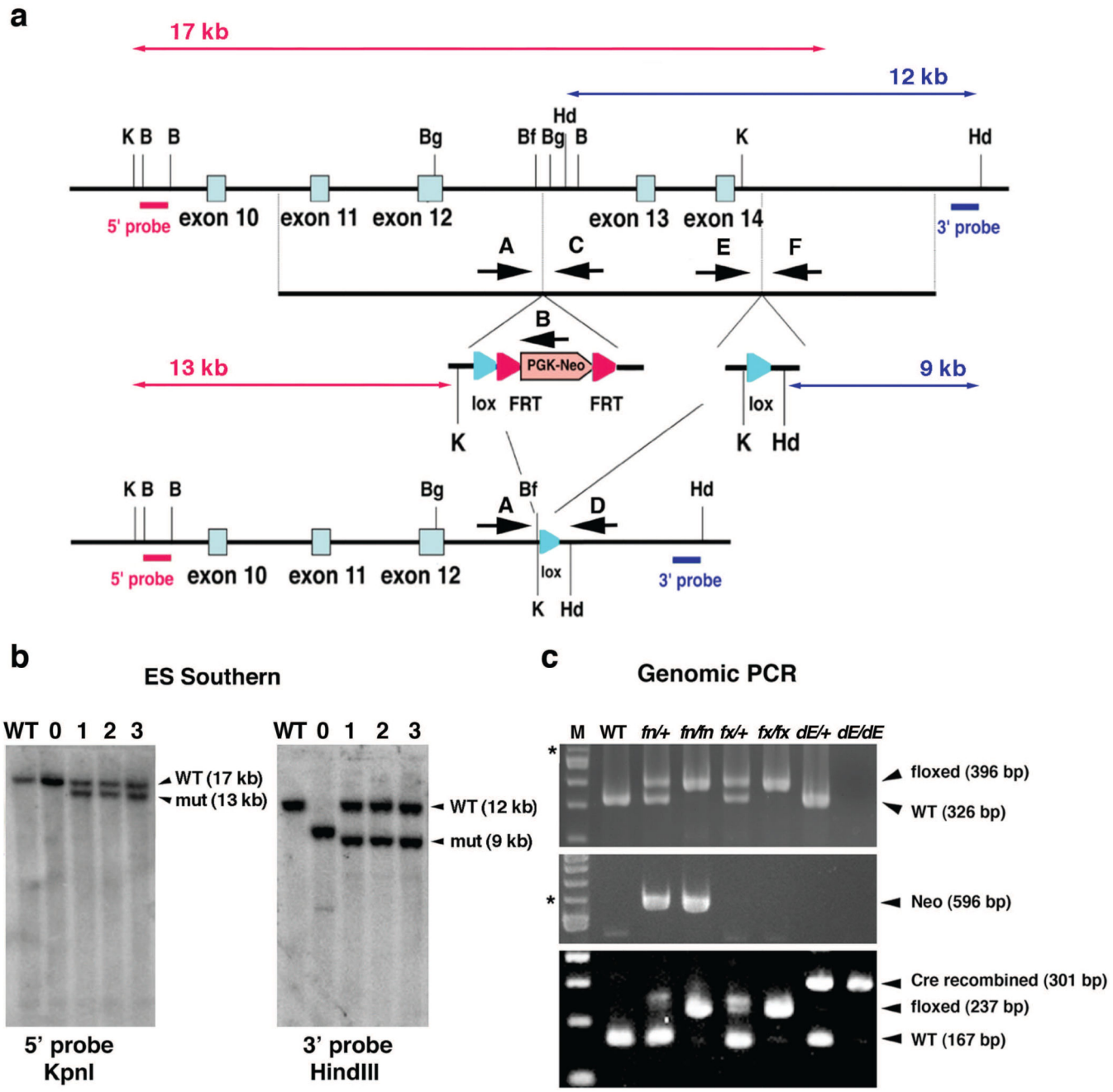

Figure 2. Generation of *Evc2/Limbin* conditional mutant mouse

(a) A loxP site followed by a *Pgk-neo* cassette flanked by FRT sites was inserted into intron 12. Another loxP site with a *Kpn*I and a *Hind*III sites was inserted into intron 14. Positions of 5' and 3' external probes for Southern analyses and the sizes of the restriction fragments detected by these probes are shown. Hd, *Hind*III; K, *Kpn*I. (b) Genomic DNA from wild type ES cells (lane WT), randomly inserted clone (lane 0) and correctly targeted clones (lane 1–3) were digested with enzymes and blots were hybridized with the probes as indicated. (c) Primers E and F were used to differentiate the targeted allele (*fn*, floxed allele with the neo cassette, or *fx*, floxed allele without the neo cassette) from WT (top). Presence of the *Pgk-*

neo cassette in the *fn* allele was confirmed by primers A and B (middle). Primers A and D were used to detect Cre-dependent recombination (*dE*, Cre recombined allele, bottom). Mixture of the primers A, E and D can differentiate WT, floxed (*fn* or *fx*), and the Cre recombined alleles (bottom). The position of primer D is similar to that of primer F, but primer F did not work with primer A. M, 100 bp ladder; *, 600 bp.

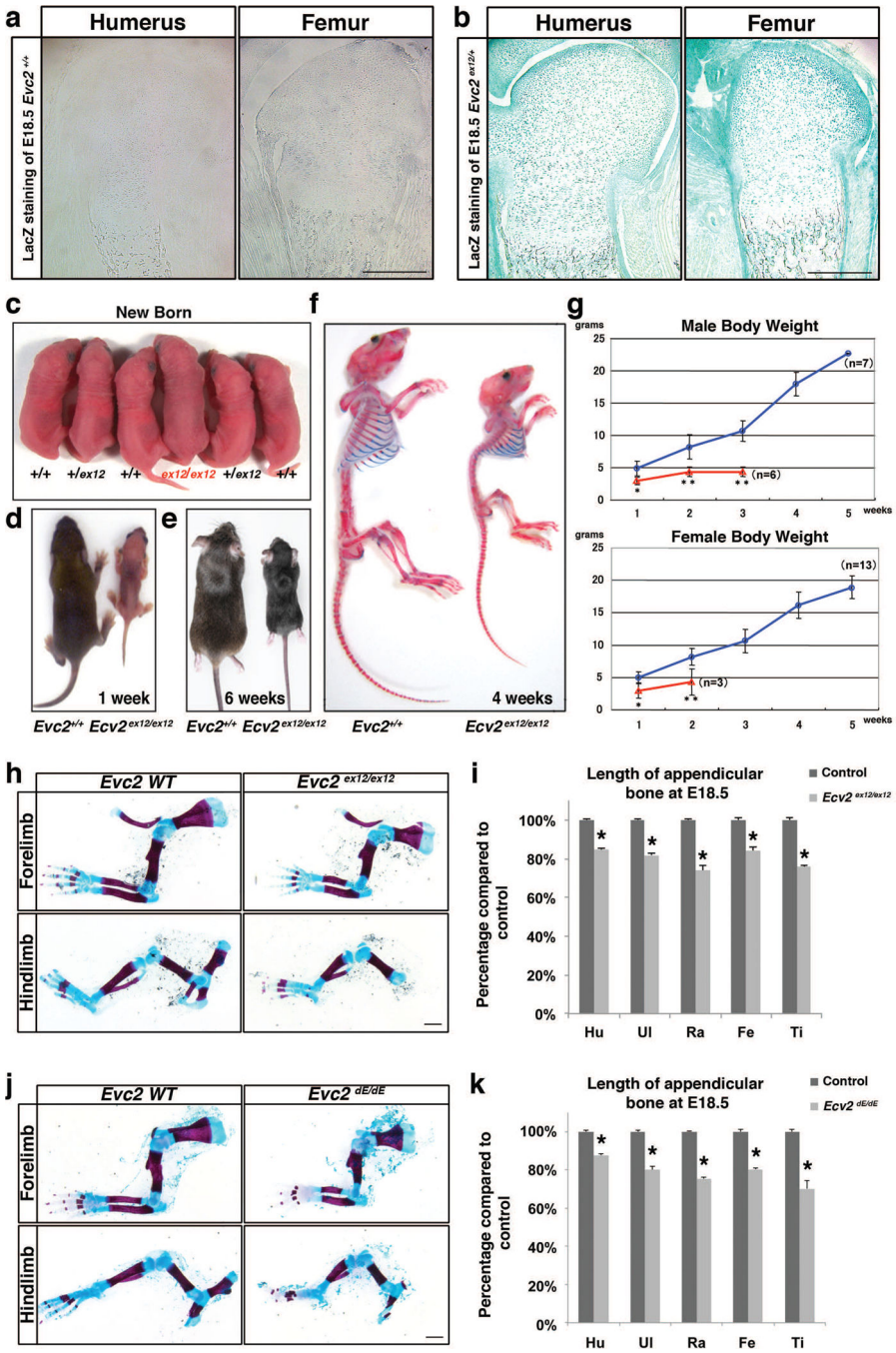

Figure 3. *Evc2* homozygous mutant mice show dwarfism

(a–b) LacZ staining showing *Evc2* expression pattern of growth plates of indicated bones from wild type (a) and heterozygous *Evc2* (b) mice. (c) Dorsal view of an $Evc2^{ex12/ex12}$ mutant mouse with littermate controls at the newborn stage. (d, e) Dorsal view of $Evc2^{ex12/ex12}$ mice with littermate controls at 1 week (d) and 6 weeks (e) after birth. (f) Side view of skeleton preparation of $Evc2^{ex12/ex12}$ and a littermate control at 4 weeks after birth. (g) Body weight gains of male and female $Evc2^{ex12/ex12}$ (red) and littermate controls (blue) were shown respectively (*, $p<0.05$, **, $p<0.01$). (h) Skeletal preparation of limbs from

E18.5 *Evc2* $^{ex12/ex12}$ and littermate control indicated shorter forelimb and hindlimb in the *Evc2* mutant. (i) Quantification of the length of indicated appendicular bone in (h) (n=10, *, $p<10^{-10}$). Hu, humerus; Ul, ulna; Ra, radius; Fe, femur; Ti, tibia. (j) Skeleton preparation of limbs from E18.5 *Evc2*$^{dE/dE}$ embryos and littermate controls indicated shorter forelimb and hindlimb in the *Evc2* mutant. (k) Quantification of the length of indicated appendicular bone in (j) (n=10, *, $p<10^{-10}$). Scale Bar: 200 um for a and b, 1 mm for h and j.

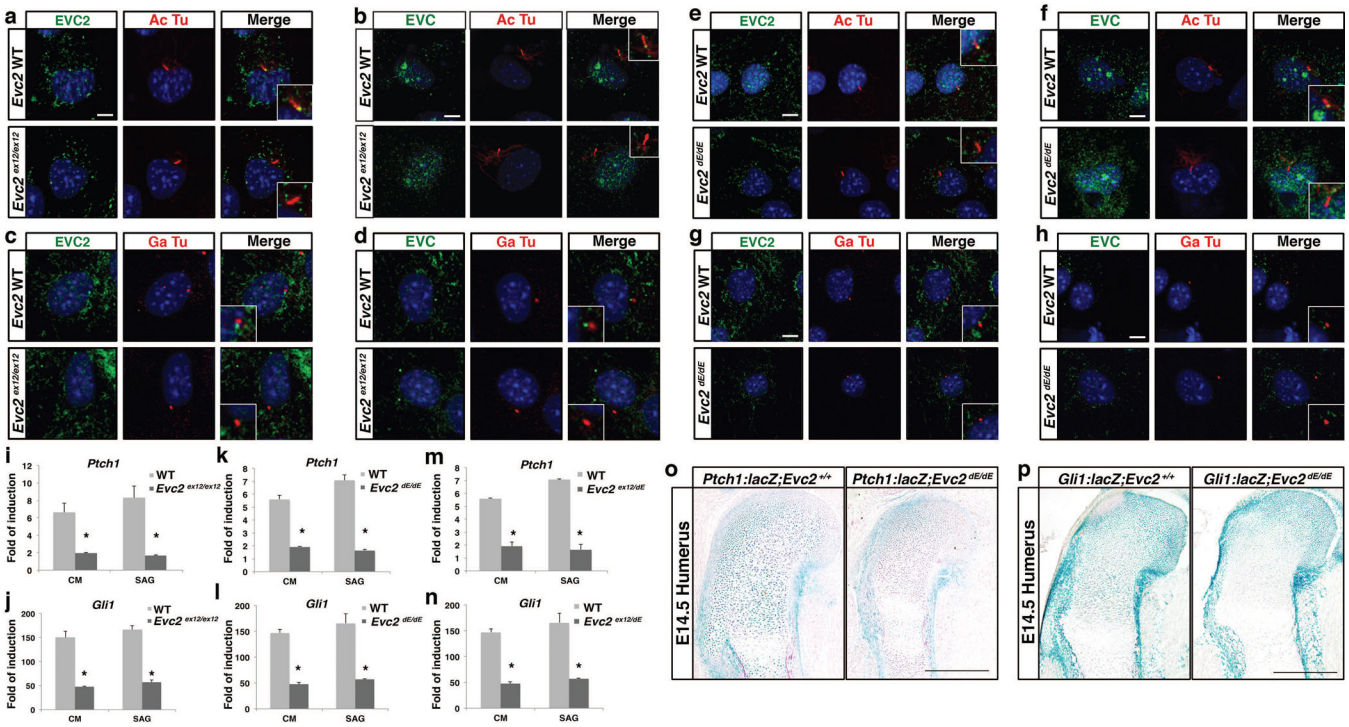

Figure 4. *Evc2* mutations result in abrogated ciliary localization and compromised Hedgehog signaling

(a–h) Immunoflorescence visualized localizations of EVC2 (a, c, e, g) and EVC (b, d, f, h) (green) within primary cilium (acetylated tubulin, Ac Tu; a, b e, f, red) or next to the centrosome (gamma tubulin, Ga Tu; c, d, g, h, red) of primary chondrocytes from $Evc2^{ex12/ex12}$ (a–d), $Evc2^{dE/dE}$ (e–h) or their littermate controls. (i–n) MEF cells from $Evc2^{ex12/ex12}$ (i, j), $Evc2^{dE/dE}$ (k, l) or $Evc2^{ex12/dE}$ (m, n) and their littermate controls were treated by Hedgehog conditioned medium (CM) or smoothen agonist (SAG). After 24 hours, expression levels of *Ptch1* (i, k, m) or *Gli1* (j, l, n) were quantified. Folds of induction were calculated using amount of RNA after treatment divided by amount of RNA with no treatment (n=3, *, $p<0.01$). (o–p) Changes in Hedgehog signaling levels in growth plates of $Evc2^{dE/dE}$ and its litter mate mice were visualized by lacZ staining after introduction of *Ptch1-lacZ* (o) and *Gli1-lacZ* (p) into the $Evc2^{dE/dE}$ background. Bar: 10 um for a–h, 200 um for o–p.

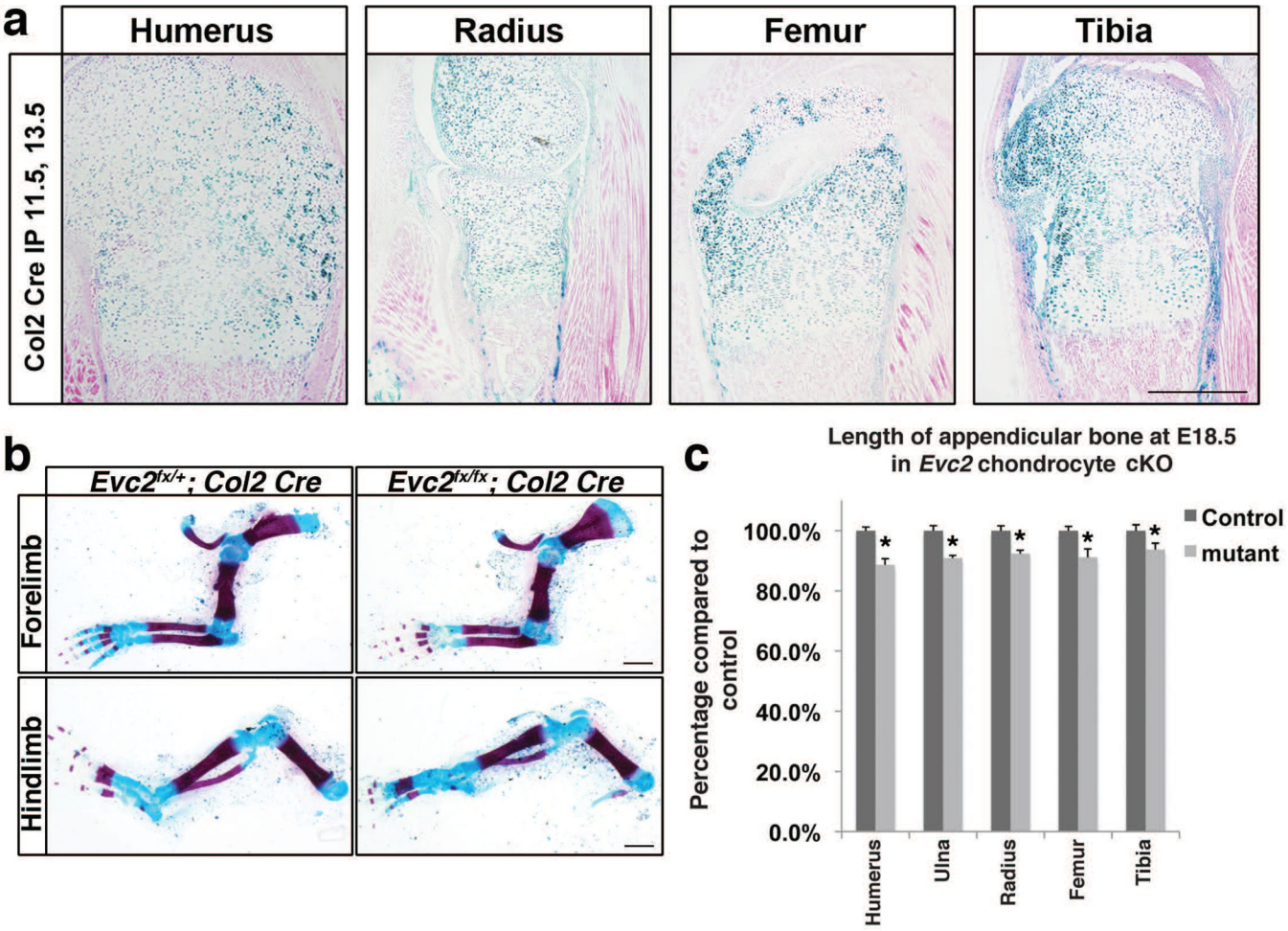

Figure 5. Similar dwarfism was observed in *Evc2* chondrocyte-specific deletion

(a) *Col2*-Cre^{ERT} was crossed with *R26R* Cre-reporter mice and tamoxifen was injected at E11.5 and 13.5. Each appendicular bone indicated above were isolated at E18.5 and stained for lacZ activity. (b) Skeleton staining at E18.5 showing appendicular bones in limbs in *Evc2* conditional mutant and littermate controls. (c) Quantification of the length of indicated appendicular bones in (b) (n=6, *, $p<10^{-5}$). Bar: 200 um for a, 1 mm for b.

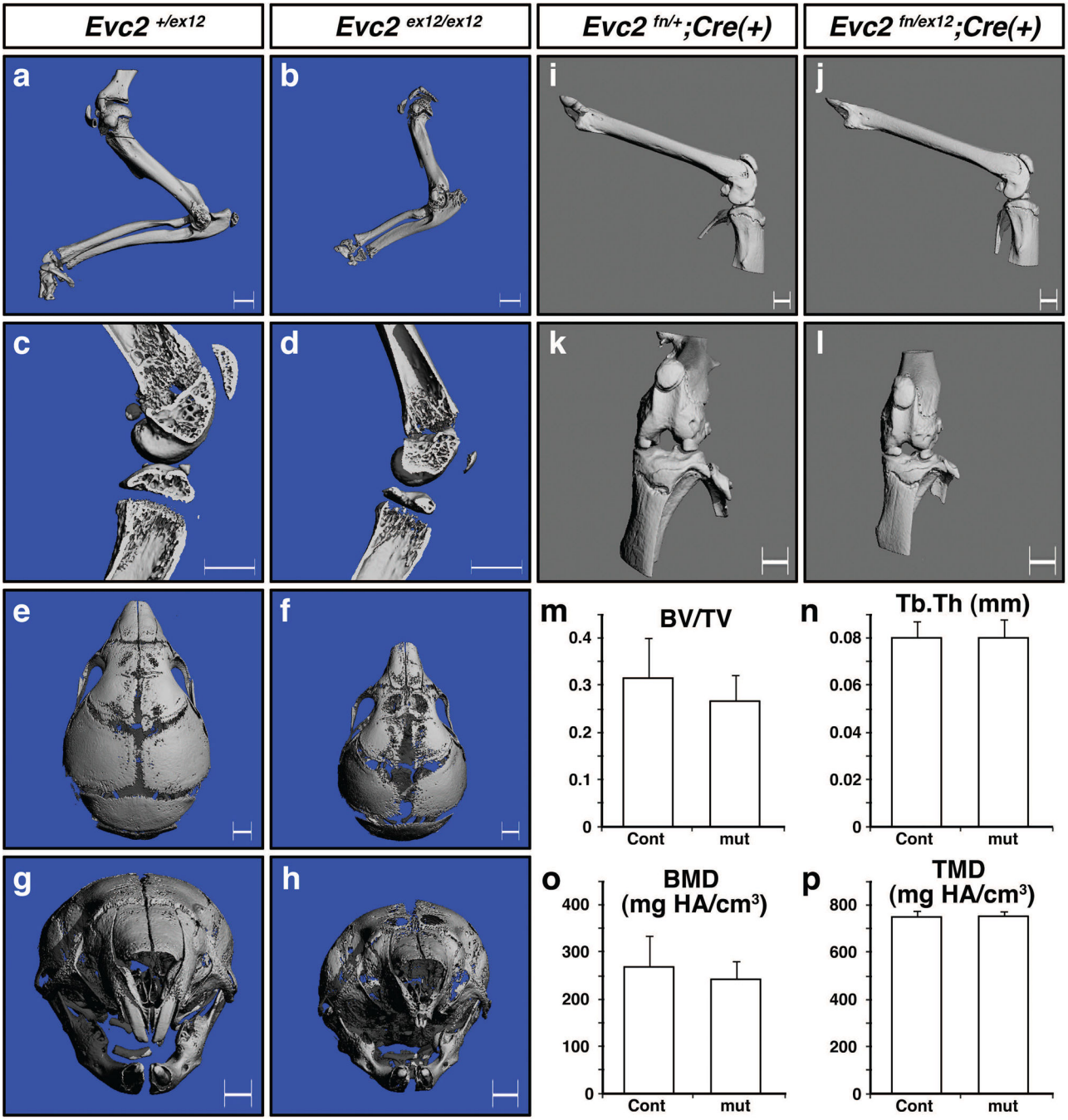

Figure 6. *Evc2/Limbin* is critical for skeletal development but dispensable for osteoblast function

(a–h) microCT images from control *Evc2*$^{+/ex12}$ and mutant *Evc2*$^{ex12/ex12}$ mice at postnatal day 6 (P6). Images from forearms (a, b), knee joints (c, d) and craniofacial regions (e–h) are shown. (i–l) microCT images of bones from osteoblast-specific knockout mice using *Osterix*-Cre at 6 months after birth. Control (*Evc2*$^{fn/+}$;*Cre*(+)) and cKO (*Evc2*$^{fn/ex12}$;*Cre*(+)) femur (i, j) and knee joints (k, l) are shown. (m–p) microCT analyses of trabecular compartments of tibia. Cont; *Evc2*$^{fn/+}$;*Cre*(+), n=11, mut; *Evc2*$^{fn/ex12}$;*Cre*(+), n= 4. BV/TV;

bone volume per tissue volume, Tb.Th; trabecular thickness, BMD; bone mineral density, TMD; tissue mineral density. Bar: 1mm.

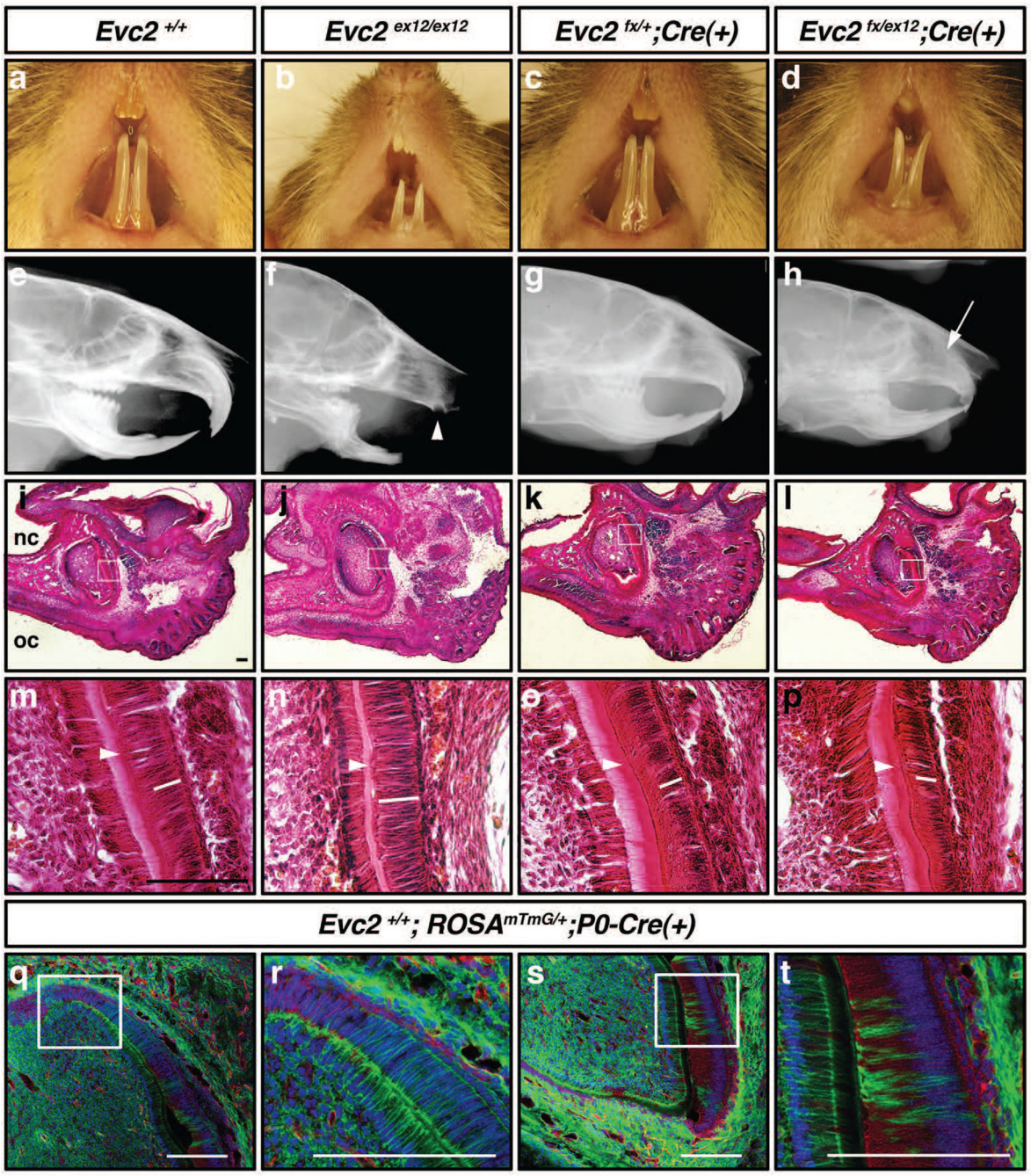

Figure 7. *Evc2/Limbin* in dental mesenchyme is critical for normal incisor growth

(a–d) External morphology of oral cavity and incisors at 6 weeks after birth. (e–h) Lateral X-ray radiograms taken at 6 weeks after birth. White arrowhead, severely reduced upper incisor in *Evc2*$^{ex12/ex12}$ mice. White arrow, posterior end of upper incisor in *Evc2*$^{fx/ex12}$*;P0*-Cre(+) mice. (i–p) Histological observation of upper incisors at E18.5. k–p show higher magnification of encircled regions in i–l. Sagittal sections, anterior is right. nc, nasal cavity; oc, oral cavity. White bars, approximate position of nucleus in ameloblasts. White arrows, deposition of dentin. (q–t) Expression patterns of Cre-reporter at E18.5. mTmG mice were

bred with *P0*-Cre and cryosections were made. Red, Td-tomato (before Cre recombination); green, GFP (after Cre recombination); blue, DAPI. Bar: 50 um.